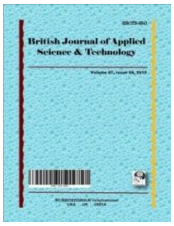

British Journal of Applied Science & Technology
9(1): 86-99, 2015, Article no.BJAST.2015.249
ISSN: 2231-0843

SCIENCEDOMAIN *international*
www.sciencedomain.org

Electrochemical Studies on Aluminium Corrosion in Dilute Alkaline Dispersions of Graphene Oxide

Pradip Kr. Ghosh[1], Susanta Ghosh[2*] and I. Basumallick[1*]

[1]Electrochemistry Laboratory, Department of Chemistry, Visva-Bharati University, Santiniketan-731235, India.
[2]Electrochemistry Laboratory, Integrated Science Education and Research Centre, Visva-Bharati University, Santiniketan-731235, India.

Authors' contributions

This work was carried out in collaboration between all authors. All the authors read and approved the final manuscript.

Article Information

DOI: 10.9734/BJAST/2015/17571
Editor(s):
(1) Jesús F. Arteaga, Department of Chemical Engineering, Physical Chemistry and Organic Chemistry, University of Huelva, Spain.
Reviewers:
(1) Anonymous, Ege University, Turkey.
(2) Anonymous, Egyptian Petroleum Research Institute, Egypt.
(3) Anonymous, I-Shou University, Taiwan.
Complete Peer review History: http://www.sciencedomain.org/review-history.php?iid=1136&id=5&aid=9212

Original Research Article

Received 18th March 2015
Accepted 24th April 2015
Published 11th May 2015

ABSTRACT

Graphene Oxide (GO) sheet with different degree of exfoliation has been prepared by modified Hummers' method. These exfoliated GO sheets have been characterized by UV–VIS, FTIR, powder XRD, Raman, Fluorescence, SAED spectroscopy and HR-TEM. Effect of GO exfoliation on Al corrosion in alkaline medium has been studied by weight loss, potentiodynamic polarization and FESEM methods. The potentiodynamic polarization and weight loss studies reveal that Al corrosion is strongly inhibited due to formation of an ultra thin film of exfoliated GO over Al surface and the inhibition effect highly depends on the degree of exfoliation of GO.

Keywords: Aluminium corrosion; graphene-oxide; exfoliation; polarization studies; inhibition.

**Corresponding author: E-mail: ibasumallick@yahoo.co.uk; Susanta.ghosh@visva-bharati.ac.in;*

1. INTRODUCTION

Recently, studies on metal corrosion have gained momentum due to increasing use of metals in different fields of technology [1,2]. Corrosion studies of aluminium have also received considerable interest because of their extensive industrial applications [3,4]. Aluminium has emerged as an alternate material after iron for many applications like; aviation, automobiles, household appliances, interconnects electrodes, integrated circuits and chemical processing industries [5]. Apart from these, Al is a low cost, abundant metallic element in the earth's crust with low density, high ductility and an excellent thermal and electrical conductivity with standard potential of 1.676 V vs. standard hydrogen electrode (SHE). More importantly, Al is highly resistive toward atmospheric corrosion due to the formation of a defensive oxide layer over it [6].

Li-ion batteries are widely used owing to their excellent energy and power densities [7-9]. However, its high cost and moisture sensitiveness compelled scientists to focus on Al systems [10-15] and thus studies on Al-air battery have been initiated to replace Li ion batteries [16,17]. But the main drawback with Al-air batteries is the rapid corrosion of Al in alkaline medium with decreased efficiency over time [18]. To reduce the corrosion rate of Al in alkaline environment, inhibitive effects of various chemical compounds and naturally occurring substances have been studied. Inorganic inhibitors like; hexa-valent chromium compounds, phosphates, borates, tungstates, molybdates, silica nanoparticles and arsenates are found useful anti-corrosive agents for Al [19-23]. But toxic and carcinogenic effects of some of these inorganic inhibitors restrict Al-air system from commercialisation. Consequently, scientists have focused on the development of environmentally friendly, cost-effective and non-hazardous corrosion inhibitors.

In this respect, Graphene is an environment friendly, low cost, chemically inert and nontoxic material. Owing to exceptional physical properties, chemical tenability and high potentiality, Graphene research has gained momentum that generates more than ten thousands publications with an accelerating rate [24]. Main advantage with Graphene is that it can easily be converted to water dispersible Grapheme Oxide (GO) by various techniques [25-37], and most of the techniques used simplified or modified Hummer method [38]. The useful property of Graphene and GO is that they can provide an anti-corrosion protection layer without affecting the electrical and optical properties of the coated surface [39-44].

In view of these useful properties, GO has been synthesized by modified Hummer's method [38] with different degree of exfoliation for the study of Al corrosion in dilute NaOH solution using weight loss, potentiodynamic polarization and FE-SEM techniques. The primary objective of the present study is to realize the effect of exfoliation on Al corrosion in dilute alkaline solution.

2. EXPERIMENTAL DETAILS

2.1 Materials and Methods

2.1.1 Synthesis of GO

For the synthesis of GO, 1g of graphite powder (Alfa Aeser, 99.9995%), and 0.5g of $NaNO_3$ (AR grade) were added into 40 ml concentrated H_2SO_4 (Merck, India, 98.0%) at room temperature. The solution was then stirred for 15 minutes in an ice-bath, followed by slow addition of 5g $KMnO_4$ (BDH, India). The rate of addition of $KMnO_4$ was controlled cautiously to avert the temperature of the suspension from exceeding 20°C. Stirring was further continued for 3 hours at < 5°C and then the ice-bath was removed and the mixture was stirred overnight for 18 hours at room temperature. The temperature of the mixture was brought to 35°C with constant stirring for another 30 minutes. The mixture gradually thickened and thus a brownish grey colour paste was obtained. 80 mL distilled water was then added into the resulting paste maintaining the temperature at >80°C for 15 minutes. The resulting solution was then cooled down to room temperature under tape water and kept for another 10 minutes. The suspension was further diluted to approximately 245 ml with distilled water, followed by addition of 40 ml 3% H_2O_2 (Merck, India). Upon treatment with H_2O_2, the suspension was turned bright yellow (Fig. 1a). The yellow suspension was filtered resulting in a yellow-brown filter cake (Fig. 1b). The filter cake was washed three times with 3% diluted HCl (Merck, India) and warm water. The produced graphite oxide was dried for few days in vacuum (Fig. 1c). GO solution (Fig. 1d) was obtained by exfoliating graphite oxide in distilled water by ultrasonication for different period of time and the samples codes with sonication time are shown in Table 1.

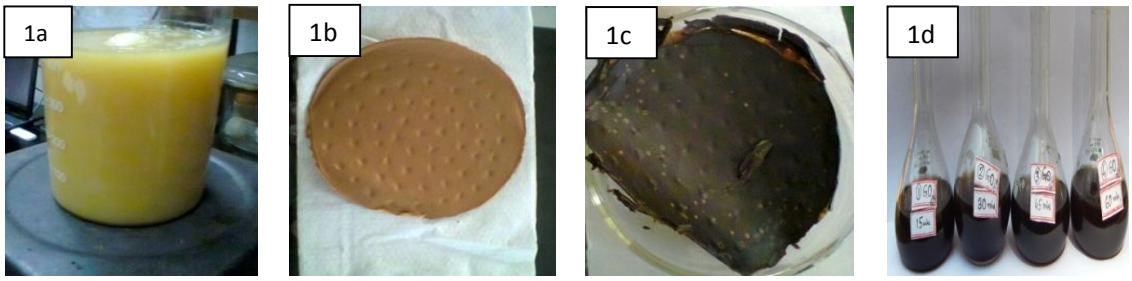

Fig. 1. (a) Bright yellow Graphite Oxide, (b) yellow brown Graphite Oxide, (c) Dried cake like Graphite Oxide and (d) Exfoliated GO solution in double distilled water

Table 1. Sample details

Sample Codes	Sonication Time (minutes)
GO1	15
GO2	30
GO3	45
GO4	60

2.1.2 Characterizations

GO was characterised by various spectroscopic techniques, such as UV-Visible spectroscopy (PerkinElmer UV/VIS spectrometer Lambda 35), Fourier Transform Infrared Spectroscopy (FTIR, 8400S PC, Shimadzu, Japan), Powder X-Ray Diffraction (XRD, Ultima IV, Rigaku, Japan, CuKα, λ= 1.5406Å), Raman spectroscopy (Microscope-BX41, TRIAX 550), Thermo gravimetric Analysis (TGA, Perkin-Elmer Sweden; model number STA 6000), Fluorescence spectroscopy (LS 55, PerkinElmer, Japan), Transmission Electron Microscopy (TEM, JEM 2100, JEOL, Japan), and Surface Area Electron diffraction (SAED, JEM 2100, JEOL).

The UV-VIS spectra were recorded in the wavelength region of 200-800 nm by dispersing sample in distilled water for the entire studies. FTIR spectra were recorded with the vacuum dried samples of GO and Graphite after preparing KBr pellets of the samples in the wave-number region of 500 - 4000 cm^{-1}. For confirmation of crystalline nature, powder XRD were performed with the solid material of GO in the region of 2θ = 5-70°, using Cu-K_α as the radiation source. Raman spectra were recorded between 1000 to 3500 cm^{-1} at λ= 488 nm, 50xL objectives lens.

TGA measurements were carried out with a heating rate of 20°C min^{-1} under air in the temperature range of 40°C to 800°C.

All the GO samples were analyzed by TEM studies in order to identify the exact morphological change of GO with different sonication time. A small droplet of the dispersed samples was added to copper grid. The samples were allowed to dehydrate for 24 hours and then TEM images were taken at a number of random positions on the Cu grid.

For corrosion studies, initial weight loss of Al was determined at 300 K in the absence and presence of different concentration of GO1, GO2, GO3, and GO4 solutions in 0.01M NaOH (Merck, India, AR grade). The Al foils (130 mg) having dimension 1 cm × 1 cm × 0.1 cm were suspended in 50 ml beakers containing 20 ml of GO solution for 5 hours. At the end of the test the foils were cautiously washed with double distilled water and acetone to reduce further corrosion and finally the dried mass of the foil were noted. The experiments were repeated thrice and the average values were recorded. The corrosion rate (C_{rate}) of Al was calculated using the relation:

$$C_{rate} = \Delta m / At \quad \text{.....} \quad (1)$$

Where, C_{rate} is the corrosion rate of Al (mg cm^{-2} h^{-1}); Δm is the corrosion weight loss of Al (mg); 'A' is the surface area of Al foils (cm^2); and 't' is the time of contact in hour. Finally, the percentage corrosion inhibition efficiency (I_W %) was calculated using the following equations:

$$I_W\,\% = 100 \times [1-(C_{rate} / C^0_{rate})] \quad \text{.....} \quad (2)$$

Where, C^o_{rate} and C_{rate} are the corrosion rates of Al in 0.01 M NaOH in the absence and presence of different concentration of GO1, GO2, GO3, and GO4 solution, respectively.

On the other hand, potentiodynamic polarization studies of high purity Al rod were performed to measure the corrosion potential (E_{corr}), corrosion current (I_{corr}), Tafel cathodic slopes (β_c), Tafel

anodic slope (β_a) of Al in 0.01 M NaOH solution in the absence and presence of different concentration of GO1, GO2, GO3, and GO4 solution using a potentiostat-galvanostat (Versastat II, PAR) at 300 K. The corrosion defence efficiency was computed from those data. The measurements were executed by exposing the Al rod (Johnson, Matthey, UK, 99.9%) of area 3.5 cm^2 as working electrode, the platinum metal as counter electrode and a saturated Calomel electrode (SCE) as reference electrode. The upper surface of Al was polished with silicon carbide (SiC) abrasive paper, washed with double distilled water and acetone and dried in warm air. Prior to each experiment, the working electrode was reserved on open circuit conditions in the electrolyte for 30 minutes to achieve equilibrium. The polarization measurements were performed over a potential range from -0.25 V to +0.25 V vs. SCE with respect to the open circuit potential (OCP) at a scan rate 0.5 mVs^{-1}. The linear Tafel segments of anodic and cathodic curves were extrapolated to find the I_{corr} values. The percentage corrosion defence efficiency (IE_D %) was calculated by using the following equation,

$$IE_D\ \% = [1 - (I_{corr} / I^0_{corr})] \times 100 \ldots\ldots\ldots\ldots \quad (3)$$

Where, I^0_{corr} and I_{corr} are the corrosion current densities of Al in 0.01 M NaOH in the absence and presence of different concentration of GO1, GO2, GO3, and GO4 solution, respectively.

The surface morphology of Al in the absence and presence of GO1 and GO3 in 0.01 M NaOH solution were analyzed by FE-SEM (ZEISS, SUPRA 55 VP) and Energy Dispersive Spectroscopy (EDX, ZEISS, SUPRA 55 VP).

3. RESULTS AND DISCUSSION

The UV-Visible spectra of four GO samples with different exfoliation are shown in Fig. 2.The patterns of all spectra are found to be similar and show two distinct absorption maxima (λ_{max}) at 230 nm and 304 nm. The first λ_{max} value is mainly due to the π→ π* transition of the C=C bond and the second one is attributed due to n→ π* transition of the carbonyl groups, which is similar to the reported values in the literature [34]. The overall absorption spectrum indicates that the larger extinction coefficient of GO due to aromatic rings remains unaltered and the degree of exfoliation does not have much effect on it.

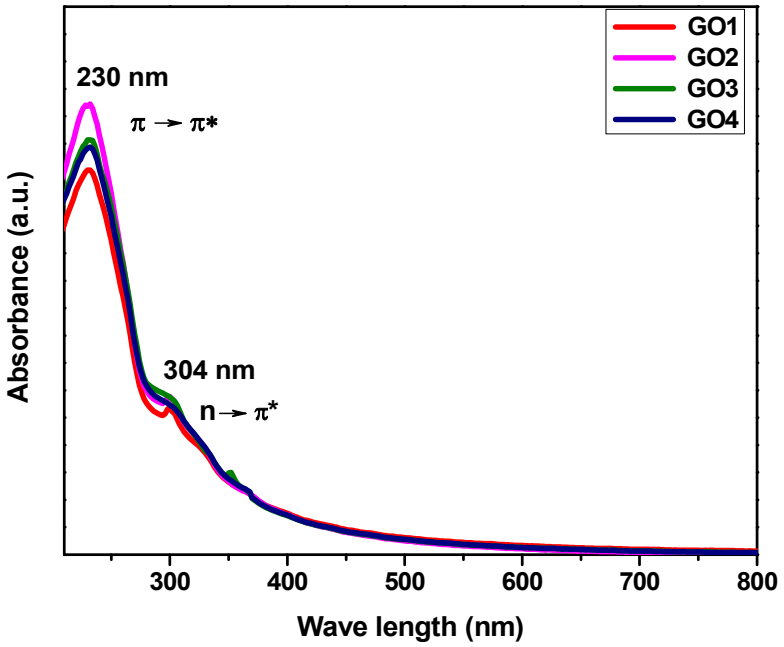

Fig. 2. UV-VIS absorption spectra of GO1, GO2, GO3 and GO4

FTIR spectra of graphite and GO are shown in Fig. 3, which was recorded to confirm the different functional groups present in graphite and GO samples. The peak at 3413 cm^{-1} is attributed due to O – H stretching, at 1722 cm^{-1} is attributed due to C = O stretching vibration, at 2355 cm^{-1} is due to symmetric and asymmetric C – H stretching mode and peaks at 1618 cm^{-1} and 1076 cm^{-1} are attributed due to C = C (from unoxidized sp^2 C=C bonds) stretching vibration and C – O vibrations of GO, respectively [33,34]. It is found that the degree of exfoliation of GO does not produce any change in FTIR spectra. Hence, the FTIR analysis corroborates the formation of GO and hygroscopic nature of the sample.

Fig. 4 shows the powder XRD patterns of graphite and GO. A distinct diffraction peak at 10.93° for GO for (001) plane and two distinct diffraction peaks at 26.47° for (002) plane and at 54.5° for (004) plane of graphite are observed. The interlayer distance values for graphite (d_{002}) and GO (d_{001}) are found to be 0.34 nm and 0.8 nm, respectively. The increase in interlayer spacing value of GO is attribute to the presence of oxygen functional groups to the carbon basal plane via chemical oxidation reaction and some other structural defects [33,44]. Therefore, the peaks signify the crystalline structure of graphite and GO.

The characteristic SAED images are shown in Fig. 5. Fig. 5 shows that a perfect six part ring patterns are observed for each sample. This is due to the crystalline environment of GO which resemble the result of powder XRD spectroscopy.

The Raman spectra of graphite and GO are shown in Fig. 6. GO shows a prominent D band at ~1350 cm^{-1} with an intensity comparable to the 'G' band at ~1587 cm^{-1} whereas, graphite shows only one 'G' band at ~1581 cm^{-1}. Raman spectra are mainly used to realize the structural properties of GO materials and it should be mentioned here that the 'G' band initiates mainly due to inplane vibration of sp^2 carbon atoms of GO and graphite samples, whereas the 'D' band arising from a breathing mode of a K- point photons of A_{1g} symmetry for GO [29,34,37]. Besides these two peaks, one additional peak arises from a two photon double resonance Raman process, known as '2D' band at 2758 cm^{-1}. Hence, it is confirmed that GO is formed successfully.

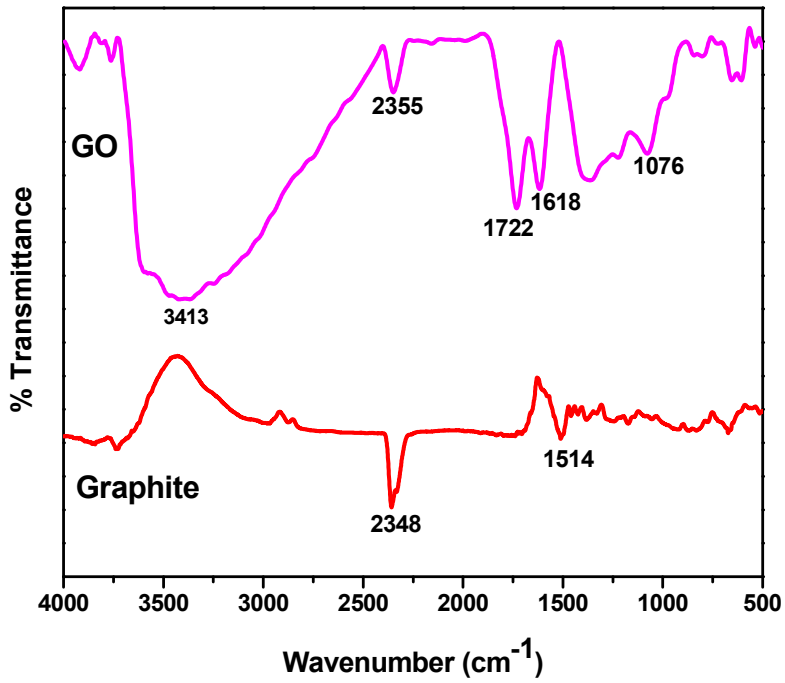

Fig. 3. FTIR spectra of graphite and GO

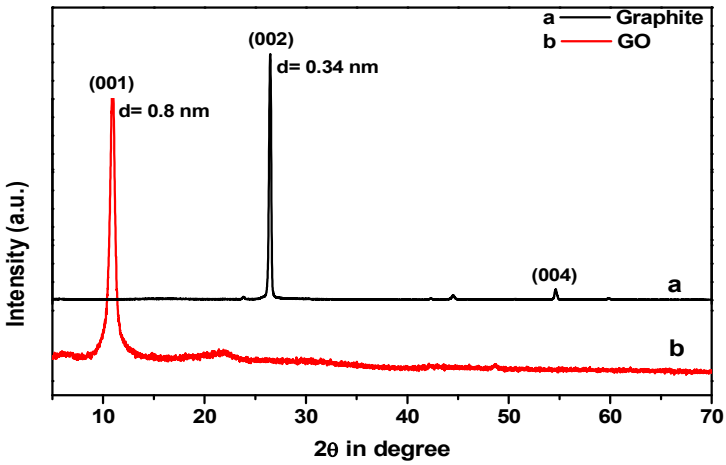

Fig. 4. Powder XRD patterns of graphite and GO

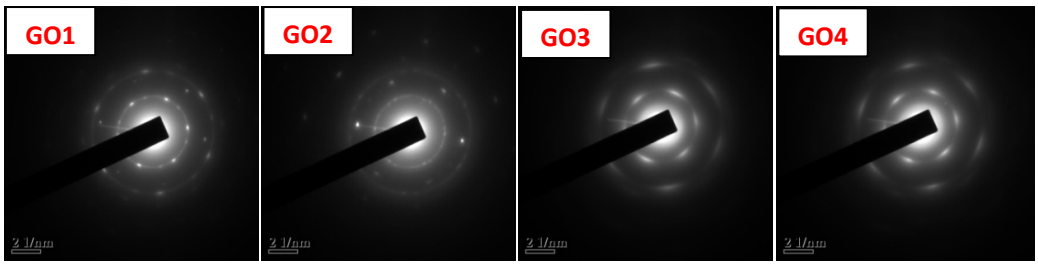

Fig. 5. SAED images of GO1, GO2, GO3 and GO4

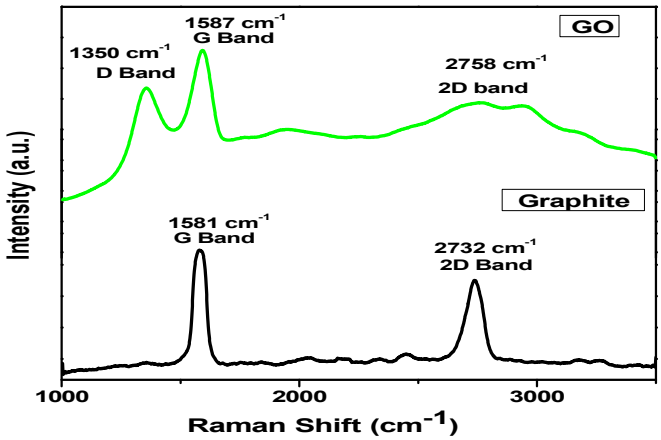

Fig. 6. Raman spectrum of graphite and GO

Thermal stability of graphite and GO were analyzed using TGA in air, as presented in Fig. 7. The TGA curves of graphite shows a very negligible weight loss around 8.5% of its total weight upto 800°C. On the other hand, GO shows constant weight loss from very beginning of the heating process, which is due to removal of adsorbed moisture, but a major weight loss is observed around 200°C with an exothermic peak quantifying a loss up to 99.3% of its total weight. The major weight loss of GO is thought to be due to pyrolysis of oxygen bearing functional groups linked with GO [34,45]. Thus TGA study clearly shows that thermal stability of GO is very less compared to graphite.

Fig. 8 represents the Fluorescence spectroscopy of GO samples. The prepared GO suspensions show slightly acidic pH (pH-5.3). Emission measured with 280 nm and 440 nm excitation at this pH shows a broad peak centred near 605 nm for GO1 but a red shift is observed with increase in degree of exfoliation [46-49]. With increasing exfoliation more water are exposed towards GO layer enhancing the polarity of the solution and thus red shift occurs.

The morphological changes upon exfoliation for different time interval are analyzed by TEM and the images are presented in Fig. 9. Fig. 9 shows that the graphite oxide particles are present in stacked form in the sample GO1. But the graphite oxide gets exfoliated to some extent to Graphene Oxides in sample GO2. However, complete exfoliation and homogenous spreading of Graphene Oxides is observed in sample GO3. In case of GO4, the structure of GO becomes agglomerate.

The percentage corrosion inhibition efficiency (I_W %) of Al foils in absence and presence of different concentration of GO samples in 0.01 M NaOH solution is illustrated in Fig.10 by weight loss measurement. It is obvious from the Fig. 10 that each GO sample acts as Al surface protector and I_W % increases with increasing concentration of each GO solution. The cause of the preferable inhibition may be due to the effective surface coverage of Al which increases by the adsorption layer of each GO solution. The maximum inhibition is observed for GO3 sample (Blue line). It may be assumed that GO3 may block the active site of Al efficiently compared to other GO samples as GO3 forms homogenous spreading colloidal dispersions. However, the inhibition efficiency for GO4 decreases due to agglomeration of the sample [37]. With increase in concentration of GO, surface coverage increases resulting enhancement of inhibition efficiency but at higher concentration of GO (fig. 10) inhibition efficiency increased to a large extent. This may be explained owing to formation of a thick layer (multi-layer) coating of GO onto Al surface which retard ion transport as well as oxygen diffusion.

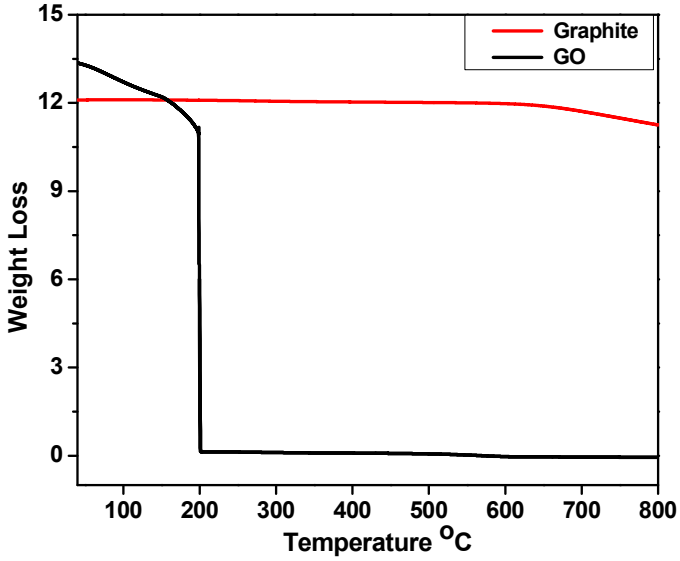

Fig. 7. TGA curves of (a) Graphite and (b) GO

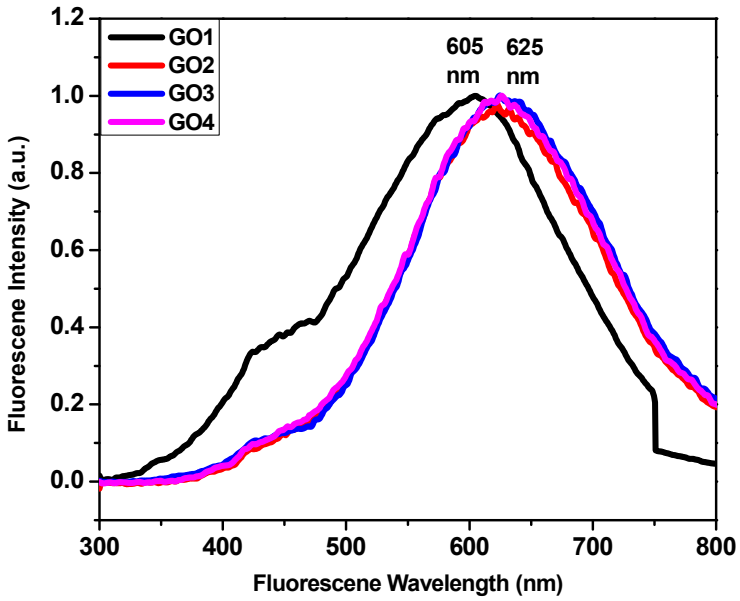

Fig. 8. Fluorescence spectra of GO1, GO2, GO3 and GO4

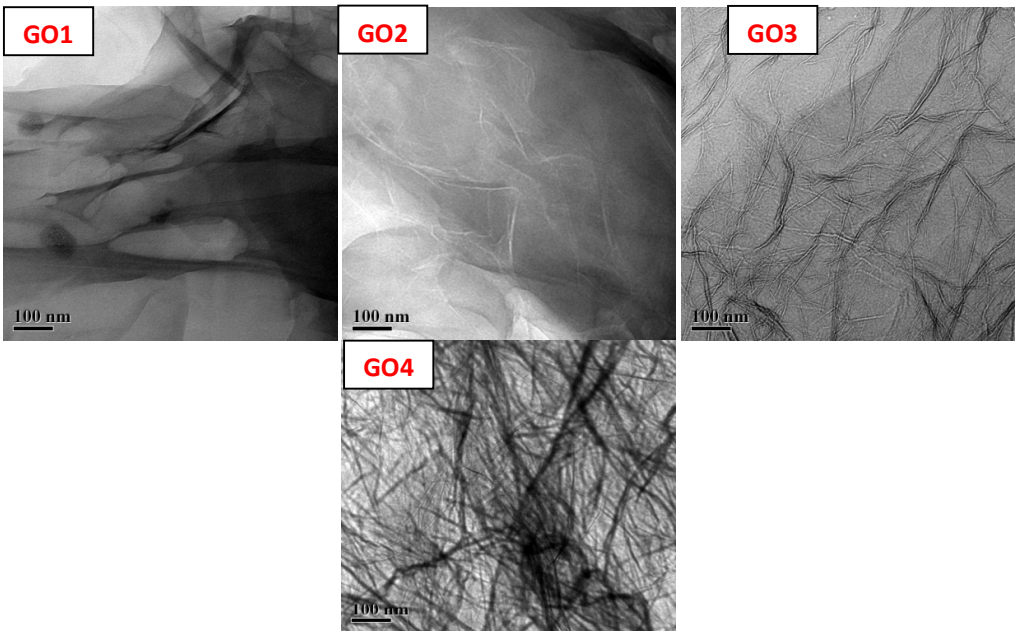

Fig. 9. TEM images of GO1, GO2, GO3 and GO4

The Potentiodynamic polarization curves are shown in Fig. 11a, 11b, 11c and 11d respectively and the corresponding corrosion kinetic parameters computed from these curves are represented in Table 2a, 2b, 2c and 2d respectively. The close inspection of all the figures and tables revealed that I_{corr} decreased noticeably with increasing concentration of each GO solution. However, the lowest value of I_{corr} was noticed for GO3 solution. Again, the E_{corr} values were almost identical with blank solution for each GO sample. This may be explained by

physical adsorption process in which the adsorbed inhibitor, GO molecules, may undergo surface reaction; producing polymeric films. Corrosion defence efficiency (IE_D%) was increased noticeably as the films grow from nearly two-dimensional adsorbed layers to three-dimensional films up to several hundred angstroms thick [50]. It was seen that GO3 was showing maximum efficiency instead of GO4, which was highest exfoliated, because GO4 undergoes agglomeration in the presence of alkaline solution and Al^{+3} ions. As GO3 sample was homogenously distributed in water medium, the polymeric films may be developed progressively enhancing the corrosion protection of Al metal in alkaline solution. The obtained IE_D % values were in agreement with the values of weight loss measurements.

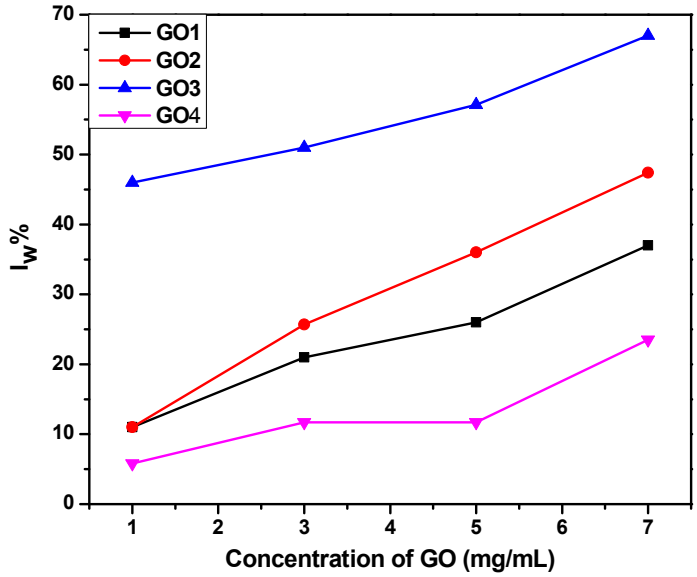

Fig. 10. I_W % of Al in presence of GO1, GO2, GO3 and GO4 samples in 0.01 M NaOH solution

Table 2a. Polarization parameters for Al in 0.01 M NaOH in the absence and presence of GO1

Sample Name	Sample's concentration (mg/mL)	$-E_{corr}$ (mV)	I_{corr} (mA/cm^2)	β_C (mV)	β_A (mV)	IE_D %
Blank		1728.7	0.3621	353.2	512.1	
GO1	1	1710.4	0.3591	382.9	465.9	8.2
GO1	3	1718.6	0.2747	285.2	384.9	24.14
GO1	5	1720.7	0.1937	314.3	291.5	46.51
GO1	7	1701.6	0.1548	232	260	57.25

Table 2b. Polarization parameters for Al in 0.01 M NaOH in the absence and presence of GO2

Sample Name	Sample's concentration (mg/mL)	$-E_{corr}$ (mV)	I_{corr} (mA/cm^2)	β_C (mV)	β_A (mV)	IE_D %
Blank		1728.7	0.3621	353.2	512.1	
GO2	1	1730.8	0.3226	318.8	480.7	10.9
GO2	3	1733.2	0.2123	262.8	334.6	41.37
GO2	5	1680	0.1463	234.5	235.9	59.6
GO2	7	1708	0.1194	227.8	186.1	67.03

Table 2c. Polarization parameters for Al in 0.01 M NaOH in the absence and presence of GO3

Sample Name	Sample's concentration (mg/mL)	$-E_{corr}$ (mV)	I_{corr} (mA/cm^2)	β_C (mV)	β_A (mV)	IE_D %
Blank		1728.7	0.3621	353.2	512.1	
GO3	1	1728.2	0.1713	197.5	244.8	52.7
GO3	3	1733.1	0.1574	217.4	213.8	56.53
GO3	5	1735.6	0.1212	142.5	131.9	66.53
GO3	7	1665.9	0.0901	148.6	155.2	75.12

Table 2d. Polarization parameters for Al in 0.01 M NaOH in the absence and presence of GO4.

Sample Name	Sample's concentration (mg/mL)	$-E_{corr}$ (mV)	I_{corr} (mA/cm^2)	β_C (mV)	β_A (mV)	IE_D %
Blank		1728.7	0.3621	353.2	512.1	
GO4	1	1706.9	0.2813	302.3	363.2	22.31
GO4	3	1724.8	0.2633	324	417.7	27.29
GO4	5	1727.6	0.2528	327.8	446	30.2
GO4	7	1671.6	0.2214	361.6	475.9	38.86

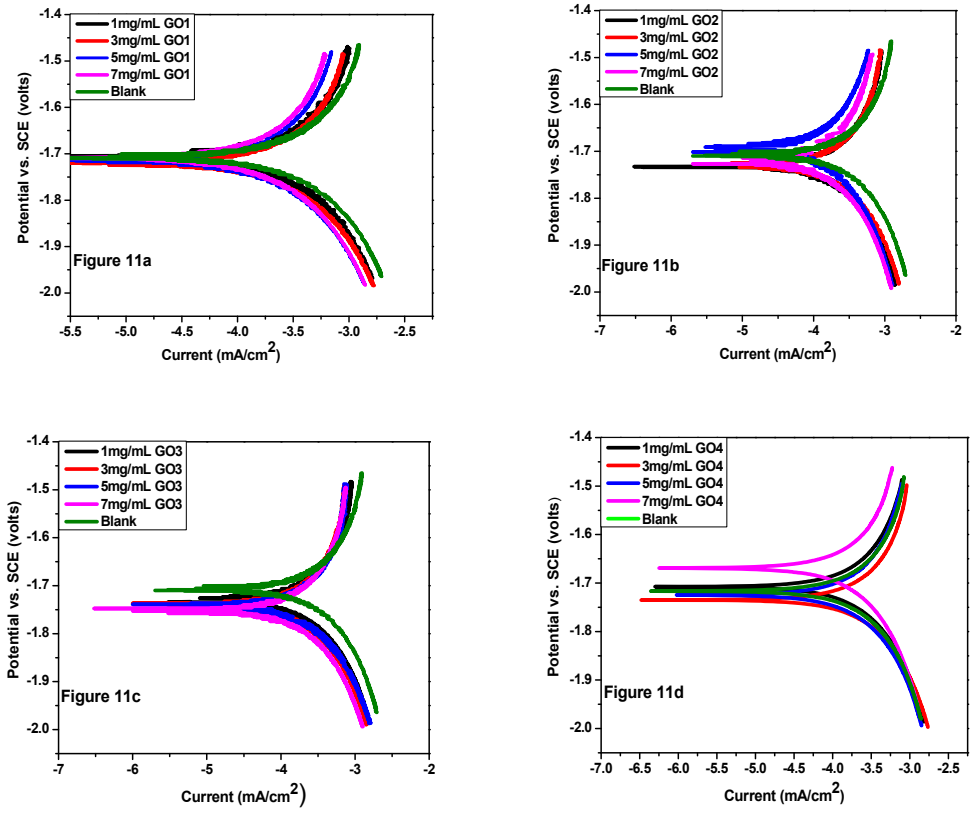

Fig. 11. Polarization curves for Al in 0.01 M NaOH in the absence and presence of GO1 (Fig. 11a), GO2 (Fig. 11b), GO3 (Fig. 11c) and GO4 (Fig. 11d), respectively

The FE-SEM images of Al immersed in 0.01 M NaOH solution in the absence and presence of GO are displayed in Fig. 12 (A), 12 (B) and 12 (C) respectively. It is clear from the images that the metal surface is robustly scratched in the absence of GO, Fig. 12(A), whereas the metal surface is less scratched with regular array in presence of GO3, Fig. 12 (C). This is credited to the formation of an improved defensive layer by GO3 compared to GO1, Fig. 12 (B). The presence of GO onto Al surface is further confirmed by EDX analysis as shown in Fig. 13 and the corresponding atomic percentage of the elements viz. C, O, Al and Si are shown in Table 3. Hence, the FE-SEM and EDX studies point out the changes of surface morphology with the rate of corrosion of Al in presence of GO in alkaline environment.

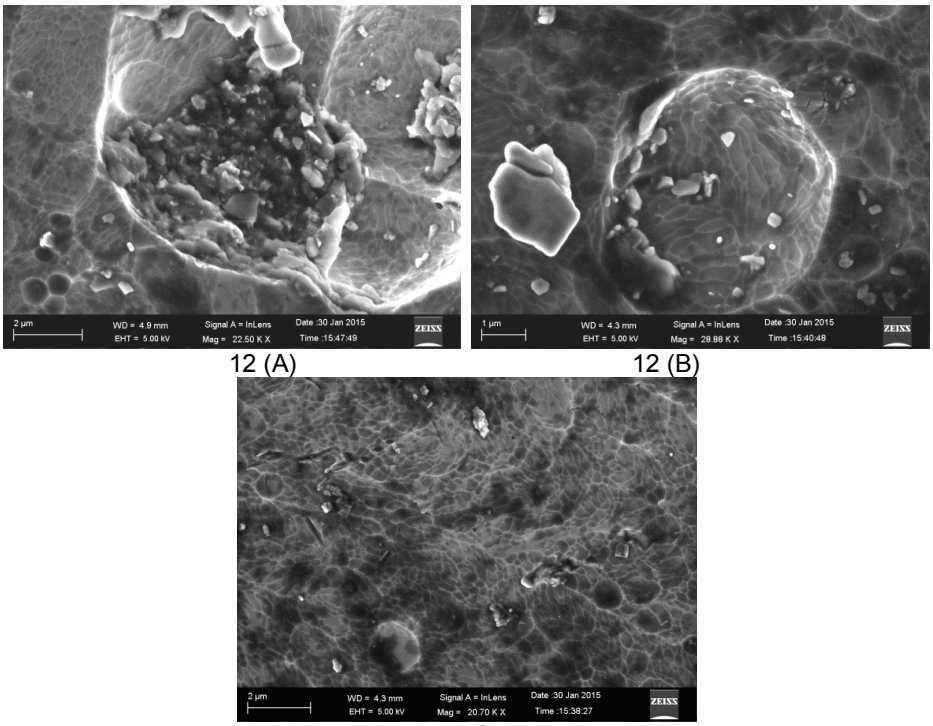

12 (A) 12 (B)

12 (C)

Fig. 12. (A) SEM image of Al metal in 0.01 M NaOH solution, (B) SEM images Al metal in presence of GO1 in 0.01 M NaOH solution and (C) SEM image of Al metal in presence of GO3 in 0.01 M NaOH solution

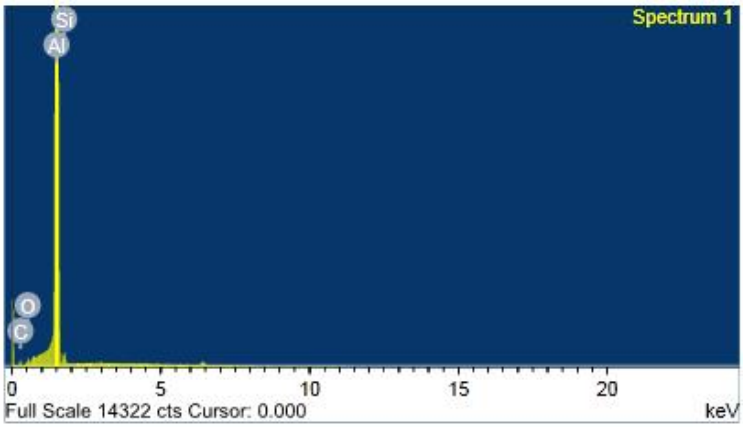

Fig. 13. EDX of Al surface in 0.01 M NaOH solution in presence of GO3

Table 3. EDX data of the the sample GO3 showing the atomic percentage of elements viz. C, O, Al and Si

Elements	Weight%	Atomic%
C K	8.29	16.73
O K	1.54	2.34
Al K	88.91	79.85
Si K	1.25	1.08
Total		100.00

Pictorial representations of GO and NaOH treated GO are shown in Fig. 14. The number of epoxy groups in GO decrease after the reaction with NaOH owing to conversion of epoxy (**–**O**–**) groups to hydroxyl (**–**OH) groups and **–**ONa groups [51] and thus GO colloid becomes negatively charged. On the other hand, Al forms Al^{3+} in alkaline solution and thus adsorbs negatively charged GO. GO colloids, containing functional groups [50] like -COOH, -OH and -O-, and having negative charge on it, act as anchoring groups to Al surface. The strength of adsorption depends on the charge on this anchoring group. The structure of the rest of the molecule influences the charge density on the anchoring group [52]. In principle, water molecules that adsorb on the Al metal surface in aqueous phase are replaced by GO. GO films are thus formed by electrostatic interactions between Al metal and the functional groups of GO. This physisorption layer hinders the anodic and cathodic reactions of corrosions.

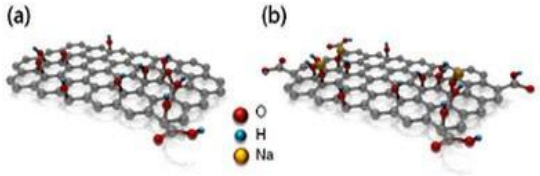

Fig. 14. Schematic representation of (a) GO, (b) NaOH-treated GO

4. CONCLUSIONS

The present study demonstrated that Graphite Oxide has been synthesized successfully by modified Hummers' method and exfoliated Graphene Oxide (GO) with different degree can be synthesized by applying an easier sonication approach. Different degree of exfoliation was confirmed by the TEM micrographs. The potentiodynamic polarization studies revealed that Al corrosions were retarded in presence of GO in dilute alkaline solution and it was observed that with increasing degree of exfoliation the corrosion inhibition efficiencies of GOs were found to increase except for the highly exfoliated sample which formed agglomerates in solution. This has been explained by physisorption of GO onto Al surface. Moreover, the verification of corrosion inhibition of GO samples onto Al metal in the aforesaid alkaline solution was evident by weight loss studies. The FE-SEM images directly showed that Al surfaces were less affected in presence of exfoliated GO solution.

ACKNOWLEDGEMENTS

The Authors are thankful to Department of Physics, Visva-Bharati University, Santiniketan, India for providing XRD facilities.

COMPETING INTERESTS

Authors have declared that no competing interests exist.

REFERENCES

1. Badaway WA, AlKharafi FM, El-Azab AS. Electrochemical behaviour and corrosion inhibition of Al, Al-6061 and Al–Cu in neutral aqueous solutions. Corros. Sci. 1999;41:709–727.
2. Vargel C. Corrosion of aluminium, Elsevier Ltd., NewYork; 2004.
3. Deepa P, Padmalatha R. Corrosion behaviour of 6063 aluminium alloy in acidic and in alkaline media. Arabian Journal of Chemistry; 2014. Available:http://dx.doi.org/10.1016/j.arabjc.2013.07.059.
4. Emregul KC, Abbas AA. The behavior of aluminum in alkaline media. Corros. Sci. 2000;42:2051-2067.
5. Ashassi-Sorkhabia H, Shabani B, Aligholipour B, Seifzadeh D. The effect of some Schiff bases on the corrosion of aluminum in hydrochloric acid solution. Applied Surface Science. 2006;252:4039.
6. Liu Z, Chong PH, Butt AN, Skeldon P, Thompson G. Corrosion mechanism of laser-melted AA2014 and AA2024 alloys. Appl. Surf. Sci. 2005;247:294-299.
7. Tarascon JM, Armand M. Issues and challenges facing rechargeable lithium batteries. Nature. 2001;414:359–367.
8. Kang K, Meng YS, Bre´gger J, Grey CP, Ceder G. Electrodes with high power and high capacity for rechargeable lithium batteries. Science. 2006;311:977–980.

9. Ge M, Rong J, Fang X, Zhou C. Porous doped silicon nanowires for lithium ion battery anode with long cycle life. Nano Lett. 2012;12:2318-2323.
10. Li C, Ji W, Chen J, Tao Z. Metallic Aluminum Nanorods: Synthesis via Vapor-Deposition and Applications in Al/air Batteries. Chem. Mater. 2007;19:5812–5814.
11. Hueso KB, Armand M, Rojo T. High temperature sodium batteries: status, challenges and future trends. Energy Environ. Sci. 2013;6:734-749.
12. Li Y, Gong M, Liang Y, Feng J, Kim J, Wang H, Hong G, Zhang B, Dai H. Advanced zinc-air batteries based on high-performance hybrid electro catalysts. Nat. Commun. 2013;4:1805.
13. Licht S, Wang B, Ghosh S. Energetic Iron (VI) Chemistry: The Super-Iron Battery. Science. 1999;285:1039-1042.
14. Cheng F, Liang J, Tao Z, Chen J. Functional Materials for Rechargeable Batteries. J. Adv. Mater. 2011;23:1695–1715.
15. Lee JS, Kim ST, Cao R, Choi NS, Liu M, Lee KT, Cho J. Metal–air batteries with high energy density: Li–air versus Zn–air. Adv. Energy Mater. 2011;1:34–50.
16. Wang W, Jiang B, Xiong W, Sun H, Lin Z, Hu L, Tu J, Hou J, Zhu H, Jiao S. A new cathode material for super-valent battery based on aluminium ion intercalation and deintercalation. Scientific reporters. 2013; 3:3383.
17. Jayaprakash N, Das SK, Archer LA. The rechargeable aluminum-ion battery. Chem. Commun. 2011;47:12610–12612.
18. Tang Y, Lu L, Roesky HW, Wang L, Huang B. The effect of zinc on the aluminum anode of the aluminum–air battery. Journal of Power Sources. 2004;138:313-318.
19. Clark WJ, Ramsey JD, McCreery RL, Frankel GS. A galvanic corrosion approach to investigating chromate effects on aluminum alloy 2024-T3. J. Electrochem. Soc. 2002;149:179-185.
20. Twite RL, Bierwagen GP. Review of alternatives to chromate for corr osion protection of aluminum aerospace alloys. Prog. Org. Coat. 1998;33:91-100.
21. El-Naggar MM. Corrosion inhibition of mild steel in acidic medium by some sulfa drugs compounds. Corrosion sci. 2007;49:2226-2236.
22. Ghosh PK, Mandal B, Ghosh S, Basumallick I. Synthesis and study of corrosion protection efficiency of silica nanoparticles on aluminium. British Journal of Applied Science & Technology. 2015;5:198-209.
23. Borisova D, Mohwald H, Shchukin DG. Mesoporous silica nanoparticles for active corrosion protection. AcsNano. 2011;5: 1939-1946.
24. Zhu Y, Murali S, Cai W, Li X, Suk JW, Potts JR, Ruoff RS. Graphene and graphene oxide: synthesis, properties, and applications. Adv. Mater. 2010;22:3906–3924.
25. Dreyer DR, Park S, Bielawski CW, Ruoff RS. The chemistry of graphene oxide. Chem. Soc. Rev. 2010;39:228–240.
26. Tang L, Li X, Ji R, Teng KS, Tai G, Ye J, Lau CWSP. Bottom-up synthesis of large-scale graphene oxide nanosheets. J. Mater. Chem. 2012;22:5676–5683.
27. Georgakilas V, Otyepka M, Bourlinos AB, Chandra V, Kim N, Kemp KC, Hobza P, Zboril R, Kim KS. Functionalisation of graphene. Chem. Rev. 2012;112:6156-6214.
28. Dimiev AM, Tour JM. Mechanism of graphene oxide formation. Acs Nano. 2014;8:3060–3068.
29. Shahriary L, Athawale AA. Graphene oxide synthesized by using modified hummers approach. International Journal of Renewable Energy and Environmental Engineering. 2014;2:58-63.
30. Huang NM, Lim HN, Chia CH, Yarmo MA, Muhamad MR. Simple room temperature preparation of high yield large area grapheme. International Journal of Nanomedicine. 2011;6:3443–3448.
31. Bykkam S, Rao VK, Chakra SC, Thunugunta T. Synthesis and characterization of graphene oxide and its antimicrobial activity against Klebsiella and Staphylococus. International Journal of Advanced Biotechnology and Research. 2013;4:142-146.
32. Hong Y, Wang Z, Jin X. Sulfuric acid intercalated graphite oxide for graphene preparation. Scientific Reports. 2013;3: 3439.
DOI: 10.1038/srep03439.
33. Song J, Wang X, Chang CT. Preparation and characterization of graphene oxide. Journal of Nanomaterials; 2014.
Available:http://dx.doi.org/10.1155/2014/276143.
34. Marcano DC, Kosynkin DV, Berlin JM, Sinitskii A, Sun Z, Slesarev A, Alemany

LB, Lu W, Tour IM. Improved Synthesis of graphene oxide. ACS Nano. 2010;4:4806-4814.
35. Cui P, Lee J, Hwang E, Lee H. One-pot reduction of graphene oxide at subzero temperatures. Chem. Commun. 2011;47: 12370–12372.
36. Huang X, Yin Z, Wu S, Qi X, He Q, Zhang Q, Yan Q, Boey F, Zhang H. Graphene-based materials: Synthesis, characterization, properties, and applications. Small. 2011;14:1876-1902.
37. Sahoo S, Hatui G, Bhatacharya P, Dhibar S, Das CK. One pot synthesis of Graphene by Exfoliation of Graphite in ODCB. Graphene. 2013;2:42-48.
38. Hummers W, Offeman R. Preparation of graphitic oxide. Journal of the American Chemical Society. 1958;6:1339.
39. Lih ETY, Zaid RM, Ling TL, Chong KF. Facile Corrosion Protection Coating from Graphene. International Journal of Chemical Engineering and Applications. 2012;3:453-455.
40. Chen S, Brown L, Levendorf M, Cai W, Ju SY, Edgeworth J, Xuesong L, Magnuson C, Velamakanni A, Piner RR, Park J, Ruoff RS. Oxidation resistance of graphene-coated Cu and Cu/Ni alloy. ACS Nano. 2011;5:1321-1327.
41. Kirkland NT, Schiller T, Medhekar N, Birbilis N. Exploring graphene as a corrosion protection barrier. Corrosion Science. 2012;56:1-4.
42. Tassel JJV, Randall CA. Mechanisms of Electrophoretic Deposition. Key Engineering Materials. 2006;314:167-174.
43. An SJ, Zhu Y, Lee SH, Stoller MD, Emilson T, Park S, Velamakanni A, An J, Ruoff RS. Thin film fabrication and simultaneous anodic reduction of deposited graphene oxide platelets by electrophoretic deposition. The Journal of Physical Chemistry Letters. 2010;1:1259-1263.
44. Ban FY, Majid SR, Huang NM, Lim HN. Graphene Oxide and Its Electrochemical Performance. Int. J. Electrochem. Sci. 2012;7:4345-4351.
45. Singh BP, Jena BK, Bhattacharjee S, Besra L. Development of oxidation and corrosion resistance hydrophobic graphene oxide-polymer composite coating on copper. Surface & Coatings Technology. 2013;232:475–481.
46. Sun X, Lui Z, Welsher K, Robinson JT, Goodwin A, Zaric S, Dai H. Nano-graphene oxide for cellular imaging and drug delivery. Nano Research. 2008;1: 203–212.
47. Luo Z, Vora PM, Mele EJ, Johnson ATC, Kikkawa JM. Photoluminescence and band gap modulation in graphene oxide. Appl. Phys. Lett. 2009;94:111909.
48. Eda G, Lin YY, Mattevi C, Yamaguchi H, Chen HA, Chen IS, Chen CW, Chhowalla M. Photoluminescence from chemically derived graphene oxide. Adv. Mater. 2010;22:505–509.
49. Galande C, Mohite AD, Naumov AV, Gao W, Ci L, Ajayan A, Gao H, Srivastava A, Weisman RB, Ajayan PM. Quasi-Molecular fluorescence from graphene oxide. Scientific Reports. 2011;1.
DOI: 10.1038/srep00085.
50. Papavinasam S. Corrosion Inhibitors, Uhlig's corrosion Handbook, second edition, ISBN 0-471-15777. 2000;5:1089-1105.
51. Lee D, Seo J. Three-dimensionally networked graphene hydroxide with giant pores and its application in supercapacitors. Scientific Reports. 2014;4.
DOI: 10.1038/srep07419.
52. Sastri VS. Corrosion Inhibitors: Principles and Application. J. Wiley, New York. 1998;39.

Peer-review history:
The peer review history for this paper can be accessed here:
http://www.sciencedomain.org/review-history.php?iid=1136&id=5&aid=9212